Available online at www.sciencedirect.com
SCIENCE DIRECT®
Bioorganic & Medicinal Chemistry 12 (2004) 2937–2950
Bioorganic & Medicinal Chemistry

Modeling and interactions of *Aspergillus fumigatus* lanosterol 14-α demethylase 'A' with azole antifungals ☆

Reena Gollapudy, Subhash Ajmani and Sudhir A. Kulkarni*

VLife Science Technologies Pvt. Ltd, 1 Akshay Residency, Plot # 50 Anand Park, Aundh Pune 411 007, India

Received 30 December 2003; revised 15 March 2004; accepted 16 March 2004
Available online 20 April 2004

Abstract—Recent identification of the sterol 14-α demethylase genes (CYP51 A and B) from *Aspergillus fumigatus* and other species by Mellado et al. (*J. Clin. Microbiol.* **2001**, *39*(7), 2431–2438), has opened up possibilities of investigating the interactions of azole antifungals with the enzyme(s) from fungi. This study describes for the first time, a model of the three-dimensional structure of *A. fumigatus* 14-α demethylase (AF-CYP51A), using the crystal structure of *Mycobacterium tuberculosis* 14-α demethylase (PDB code:1EA1) as a template. The paper also describes the various interactions between azole antifungals and the target from *A. fumigatus* (AF-CYP51A). Quantitative evaluation of these interactions is done using COMBINE analysis to understand contributions of active site residues to ligand activity. It also provides explanation for the activity/inactivity of different ligands for AF-CYP51A.
© 2004 Elsevier Ltd. All rights reserved.

1. Introduction

Opportunistic and invasive fungal infections have increased dramatically in recent years to become important causes of morbidity and mortality. *Candida* and *Aspergillus* sp. are the most infamous fungal pathogens that account for majority of invasive and opportunistic fungal infections, respectively, occurring worldwide. Currently available antifungal drugs for such infections predominantly target sterol 14-α demethylase (azoles), ergosterol (polyenes), and beta-1,3-glucan synthase (echinocandins) among others.[1–4] The first is a fungistatic target vulnerable to resistance development; the second, while a fungicidal target, is not sufficiently different from the host to ensure high selectivity. The third is a fungistatic (*Aspergillus*) or fungicidal (*Candida*) target, has limited activity spectrum and potential host toxicity that might preclude dose escalation.[1] Limitations as stated above are preventing the development of more effective antifungals. A detailed investigation of sequence and structure properties of drug targets from these pathogenic fungi may help in the development of more effective and broad spectrum antifungals.

The first class of compounds, the azoles inhibit the ergosterol biosynthetic pathway. They specifically inhibit the demethylation of precursor sterols, viz. lanosterol at position 14 by sterol 14-α demethylase (CYP51). This enzyme belongs to a superfamily of mono-oxygenases called cytochrome P450, members of which are involved in various biosynthetic functions. The chemical families that inhibit C-14 demethylation are the imidazoles and the triazoles.[2] Two classes of resistance mechanisms to these drugs operate in filamentous fungi; altered affinity of CYP51 due to target site mutation and decreased accumulation of drugs due to enhanced energy dependent drug efflux.

Since the crystal structure of CYP51 enzyme for species of *Candida* has not been obtained, different templates have been used in the literature for modeling of CYP51 of *Candida albicans* (CA-CYP51).[5–7] The model of CA-CYP51 based on three template geometries of prokaryotic microorganisms, viz.; P450cam, P450terp, P450eryF, and P450BM3 was reported along with docking of some azoles in the active site.[5] Macchiarulo et al.[6] used the crystal structures of *Mycobacterium tuberculosis* (MT-CYP51)[8] in complex with fluconazole and 4-phenylimidazole to build the CA-CYP51 model.

Keywords: *Mycobacterium tuberculosis*; *Aspergillus fumigatus*; Antifungal azoles; Molecular modeling; Docking.
☆ Supplementary data associated with this article can be found in the online version, at doi:10.1016/j.bmc.2004.03.034
* Corresponding author. Tel./fax: +91-20-2588-6737; e-mail: sudhirk@vlifesciences.com

0968-0896/$ - see front matter © 2004 Elsevier Ltd. All rights reserved.
doi:10.1016/j.bmc.2004.03.034

A model of CA-CYP51 built by chimeric substitution of active site residues of MT-CYP51 has also been reported[7] and interaction of azoles with active site residues have been pointed out.

Mellado et al.[9] have recently reported the identification of two different 14-α lanosterol demethylase-related genes (CYP51A and CYP51B) in *Aspergillus fumigatus* and other *Aspergillus* species. This is the first report of the existence of two homologous genes coding for 14-α sterol demethylase in the fungal kingdom.[9] Characterization of the CYP51 proteins (A and B) from *Aspergillus* sp. will contribute to a better understanding of azole–receptor interactions and could shed light on the structural basis, if any, for resistance mechanisms in *Aspergillus* sp.

For an in-depth understanding of variations in CYP51 of different fungal species, their structural information, either theoretical or experimental should be available. To best of our knowledge there are no reports of theoretical models of CYP51 enzymes A and B of *A. fumigatus*. The present investigation attempts to explore various interactions of azole antifungals with the lanosterol 14-α demethylase 'A' enzyme from *A. fumigatus*. A sequence and structure based comparison has also been attempted between MT-CYP51 (PDB code: 1EA1); the reported CA-CYP51 model[5,6] and the built *Aspergillus* 'A' model. This paper further attempts to compare active sites of MT-CYP51; CA-CYP51 and CYP51 enzymes A and B of *A. fumigatus*.

2. Methodology

As described in the introduction above, active site comparisons between CA-CYP51 and *A. fumigatus* CYP51A and CYP51B (AF-CYP51A and AF-CYP51B) models could shed more light on their specific interactions with azole antifungals. In order to do such an analysis, a first-level sequence comparison of the amino acid sequences of CA-CYP51 and AF-CYP51A and AF-CYP51B, was done to highlight similarities and differences in the active site regions of all the three gene products. The sequences considered for the analysis were;

Sequence 1: gi|13400014|pdb|1EA1|A
455 aa (MT-CYP51)
Sequence 2: gi|1169073|sp|P10613|CP51_CANA
528 aa (CA-CYP51)
Sequence 3: gi|14861413|gb|AAK73659.1|
515 aa (AF-CYP51A)
Sequence 4: gi|14861415|gb|AAK73660.1|
524 aa (AF-CYP51B)

The multiple alignment of sequences was performed using the CLUSTAL algorithm,[10] to identify regions of conservation, variation, and the nature of mutations/substitutions. The sequences were optimally aligned taking into consideration the reported transmembrane domains, predicted secondary structure of each of the sequences, ligand binding residues, reported access channel residues, mutation hotspots, and residues important for enzymatic activity. An active site residue analysis was performed to delineate the possible role of residues in interactions with azole antifungals.

2.1. Model building

Although the multiple alignment was performed on four sequences, the tertiary structure model of the translated gene product of *A. fumigatus* CYP51A,[9] gi: 14861413, is being reported. The recently reported crystal structure of *M. tuberculosis*, (PDB entry 1EA1[8]), 14-α demethylase was the scaffold on which the AF-CYP51A enzyme was modeled.

The sequences of cytochrome P450 14-α demethylases of *M. tuberculosis* (MT-CYP51) and of *A. fumigatus* (AF-CYP51A) were aligned using the pair-wise BLAST algorithm.[11] The Blosum-62 matrix was used with a gap penalty of 1. Secondary structure prediction was done using the JPRED server.[12] The secondary structure predictions were used to optimize the sequence alignment prior to model building, so that the accuracy of the model would be increased. An alignment of key conserved structural residues charted out the structurally and functionally important conserved regions such as the Cys-pocket. The final alignment spanned residues W32 to K515. The first 31 residues were predicted to constitute the membrane-spanning region, and therefore were not included in the final alignment and model building.

The three-dimensional model of the *A. fumigatus* CYP51A protein was built using SYBYL v6.9.[13] The strategy used for building included use of the MT-CYP51 backbone as a starting structure, upon which the side chains of the protein from *A. fumigatus* were modeled. The geometry of the conserved residues was preserved, while that of residues, which were mutated, was allowed to evolve in energetically favored conformations. Coordinates for residues in loops were extracted by a homology search with the PDB database for compatible fragments. This method threw up several candidate loops from the database whose anchor regions had a good geometric fit to the anchor regions of the model thus preserving the nearly ideal covalent geometry. Loop analysis was used to select the final compatible loop based on the quality of fit of the anchor regions, sequence homology and steric interactions. The model was then minimized using the MMFF94 force field[14] and MMFF94 charges until a rms gradient energy of 0.1 kcal/mol·Å had been achieved. During the optimization procedure, the structure was checked periodically by Ramachandran plots and other validation methods.[15]

2.2. Docking of ligands

The azole ligands chosen for docking in AF-CYP51A were selected from literature (cf. Chart 1).[16] A systematic conformational search was performed to obtain the low energy conformations of the ligands. The conformations thus obtained, were optimized till they reached

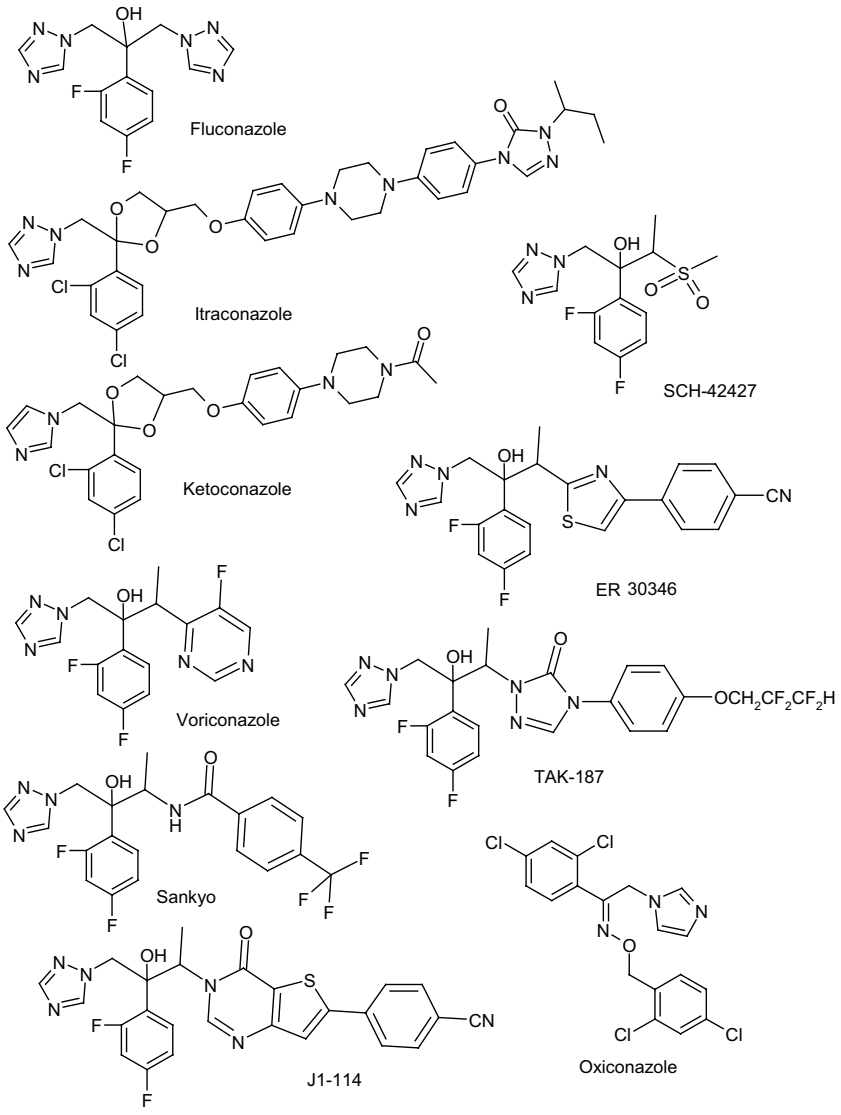

Chart 1. Antifungal azoles used in this study.

a rms gradient energy of 0.001 kcal/mol·Å. In order to define ligand–receptor interactions, docking of all the low energy conformations within a range of 5 kcal/mol from the lowest energy conformation of each molecule, into the AF-CYP51A model was done by positioning the azole molecules appropriately in the channels C1 and C2. The complexes were then minimized using the MMFF method, till they reached a rms gradient of 0.1 kcal/mol·Å. The initial positioning of the ligands was done by the keeping the N4 of the aligned molecules at a distance of ~2.37 Å from the Fe of the porphyrin ring and at an angle of ~180° w.r.t. N4–Fe–S (of Cys 454). The heme molecule was kept planar and constrained along with Fe atom during the optimization. Fe atom was kept free (nonbonded) as MMFF94 force field does not support bonding energy terms for Fe. The above procedures were performed using the MDS1.0 package.[17] The binding energy in kcal/mol or the ligand–receptor interaction energy obtained after docking the ligands into the enzyme active site can be defined as: $E_{\text{bind}} = E_{\text{complex}} - (E_{\text{receptor}} + E_{\text{ligand}})$.

2.3. COMBINE analysis

Ligand–receptor interaction energies calculated using molecular mechanics may or may not correlate well with reported ligand activity. Ligand–receptor interactions therefore could be better understood by a comparative binding energy (COMBINE) analysis. COMBINE analysis is a kind of receptor-dependent analogue method to CoMFA.[18] For each of the ligands under consideration, intermolecular and intramolecular energies are calculated for the ligand–receptor complexes, the unbound ligands and the receptor, using the MMFF94 force field. The total ligand–receptor interaction energy was partitioned into individual residue contributions, based upon electrostatic and van der Waals energy terms in the COMBINE analysis. Also another approach for COMBINE analysis was used in this study, in which difference of electrostatic and steric energy of individual residue before and after docking was used as the descriptor for building QSAR model. Residues falling in 10 Å radius from the aligned

set of ligands (in docked complexes) were considered for COMBINE analysis.

Both the approaches provide derivation of QSAR equations between experimental biological activities and a selected set of the energy terms. The QSAR model thus developed enabled identification of important residues that play a key role in ligand–receptor interaction and could provide guidelines for more effective ligand design.

Electrostatic and steric energy contribution descriptor for each residue in two COMBINE approaches was calculated as follows:

Approach I

Electrostatic:

$$\Delta E_{\text{ele}}(\text{Res}) = E_{\text{ele}}^{\text{complex}}(\text{Res} + \text{Ligand}) - [E_{\text{ele}}^{\text{enzyme}}(\text{Res}) + E_{\text{ele}}(\text{Ligand})]$$

where $\Delta E_{\text{ele}}(\text{Res})$ = electrostatic energy contribution of residue, $E_{\text{ele}}^{\text{complex}}(\text{Res} + \text{Ligand})$ = electrostatic energy of the residue and ligand in the complex, $E_{\text{ele}}^{\text{enzyme}}(\text{Res})$ = electrostatic energy of the residue in enzyme, $E_{\text{ele}}(\text{Ligand})$ = electrostatic energy of ligand.

Steric:

$$\Delta E_{\text{ste}}(\text{Res}) = E_{\text{ste}}^{\text{complex}}(\text{Res} + \text{Ligand}) - [E_{\text{ste}}^{\text{enzyme}}(\text{Res}) + E_{\text{ste}}(\text{Ligand})]$$

where $\Delta E_{\text{ste}}(\text{Res})$ = steric energy contribution of residue, $E_{\text{ste}}^{\text{complex}}(\text{Res} + \text{Ligand})$ = steric energy of the residue and ligand in the complex, $E_{\text{ste}}^{\text{enzyme}}(\text{Res})$ = steric energy of the residue in enzyme, $E_{\text{ste}}(\text{Ligand})$ = steric energy component of ligand.

Approach II

Electrostatic:

$$\Delta E_{\text{ele}}(\text{Res}) = E_{\text{ele}}^{\text{complex}}(\text{Res}) - E_{\text{ele}}^{\text{enzyme}}(\text{Res})$$

where $\Delta E_{\text{ele}}(\text{Res})$ = electrostatic energy contribution of residue, $E_{\text{ele}}^{\text{complex}}(\text{Res})$ = electrostatic energy of the residue in complex, $E_{\text{ele}}^{\text{enzyme}}(\text{Res})$ = electrostatic energy of the residue in enzyme.

Steric:

$$\Delta E_{\text{ste}}(\text{Res}) = E_{\text{ste}}^{\text{complex}}(\text{Res}) - E_{\text{ste}}^{\text{enzyme}}(\text{Res})$$

where $\Delta E_{\text{ste}}(\text{Res})$ = steric energy contribution of residue, $E_{\text{ste}}^{\text{complex}}(\text{Res})$ = steric energy of the residue in complex, $E_{\text{ste}}^{\text{enzyme}}(\text{Res})$ = steric energy of the residue in enzyme.

To evaluate statistical significance of QSAR model for an actual data set, we have employed a one-tail hypothesis testing.[18b] The robustness of the QSAR models for experimental training sets was examined by comparing these models to those derived for random data sets. Random sets were generated, by rearranging biological activities of the training set molecules. The significance of the models obtained is based on calculated Z-score.[18b]

3. Results and discussion

3.1. Bioinformatic analysis and active site prediction

Amino acid sequences of MT-CYP51, AF-CYP51A, AF-CYP51B, and CA-CYP51 were obtained from the *ENTREZ* database.[19] A CLUSTAL multiple alignment of the sequences in Pearson format was generated and is shown in Figure 1. This multiple alignment helped to delineate regions of sequence conservation and variation across all the four species. For model building, a pairwise sequence alignment of MT-CYP51 and AF-CYP51A was done and is given as Supplementary information.

A pairwise alignment of all the sequences with each other provides measures of similarities and identities as shown in Table 1. The fungal species have greater similarities and identity scores amongst each other, than with MT-CYP51. Further, AF-CYP51A and AF-CYP51B have the same identity and similarity scores against MT-CYP51 in spite of having different amino acid composition. A detailed modeling study on both the 'A' and 'B' gene products may therefore shed light on the differences and/or similarities between them at a structural level.

Based on structural information of the MT-CYP51 active site and sequence information of the other three proteins, putative active site residues in CA-CYP51, AF-CYP51A, and AF-CYP51B, were identified as shown in Table 2. The selection of active site residues in the reference protein (viz.; MT-CYP51), was done by identifying residues in the substrate binding cavity and within 8 Å from the heme.

Few significant observations made from the analysis of Table 2 are (analysis is presented with reference to CA-CYP51 sequence):

a. Residues E141, L204, G308, H310, S312, W318, H373 of CA-CYP51 are conserved across all the four gene products. Therefore, they need to be further examined for their structural conservation across all four species.
b. Residues L139, M140, K144, F145, M306, S314 of CA-CYP51 are conserved across the fungal species and vary in MT-CYP51.
c. Residues I304, G307, T311, L376, V510 of CA-CYP51, vary between *C. albicans* and *A. fumigatus*, but are conserved between AF-CYP51A and AF-CYP51B.
d. Residues T315 and P375 of CA-CYP51 warrant special investigation. T315 in *C. albicans* (which has been replaced by I301 in *A. fumigatus* CYP51A and remains T315 in CYP51B, respectively) has been shown to be associated with development of fluconazole resistance.[20] Edlind et al.,[20] observed that 'the presence of Ile at this position is apparently not significantly detrimental to *A. fumigatus* CYP51 activity, but may similarly reduce azole inhibition'. In case of AF-CYP51A, T315 is substituted by I301, which could be responsible for reduced

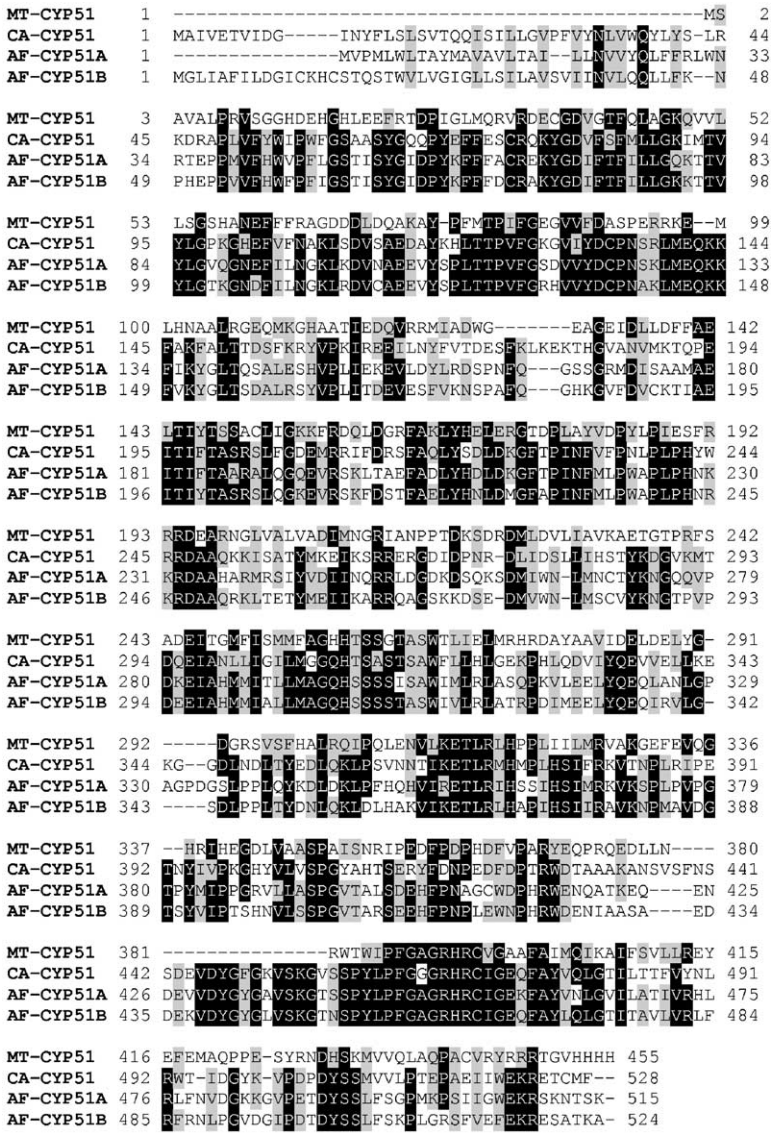

Figure 1. Multiple alignment of the sequences listed in Section 2. The shaded regions represent conserved residues. The conserved residues are colored black. Gaps are represented by dashes. The notation to the left of the sequences lists the accession numbers of the sequences. Numbers to the right and left of the sequences are the amino acid numbers.

Table 1. Correlation matrix depicting similarities and identities between the four sequences considered in this study[a] (all values are in percentages)

	MT-CYP51	CA-CYP51	AF-CYP51A	AF-CYP51B
MT-CYP51	100 (100)	—	—	—
CA-CYP51	40 (22)	100 (100)	—	—
AF-CYP51A	46 (26)	65 (47)	100 (100)	—
AF-CYP51B	49 (31)	65 (47)	76 (63)	100 (100)

[a] Values in parenthesis are the identities and open values are similarities.

fluconazole activity in *A. fumigatus*. On the other hand, AF-CYP51B retains the threonine residue. Analogously, P375 in CA-CYP51 that is represented by P372 in AF-CYP51B is mutated to S363 in AF-CYP51A. Therefore, S363 may be a candidate for site-directed mutagenesis and activity testing to determine its contribution to biological activity. Further, it remains to be determined by structure comparisons, if a conformational change has been induced by such a residue replacement.

e. Residues A146 and M374 of CA-CYP51, are changed across all the four gene products under study (cf. Table 2).

Table 2. Active site residues 8 Å from porphyrin ring of heme in all the four gene products under study[a]

M. tuberculosis	*C. albicans*	*A. fumigatus* CYP51A	*A. fumigatus* CYP51B
Y76	Y118	Y107	Y122
R96	L139	L128	L143
K97	M140	M129	M144
E98	E141	E130	E145
M99	K144	K133	K148
L100	F145	F134	F149
H101	A146	I135	V150
L152	L204	L190	L205
M253	I304	L290	L304
F255	M306	M292	M306
A256	G307	A293	A307
G257	G308	G294	G308
H259	H310	H296	H310
T260	T311	S297	S311
G263	S314	S300	S314
T264	T315	I301	T315
W267	W318	W304	W318
H318	H373	H361	H370
P319	M374	S362	A371
P320	P375	S363	P372
L321	L376	I364	I373
V435	V510	S496	S504

[a] The table highlights similarities and differences in the amino acid composition of the active sites from the three organisms being examined.

3.2. Model building

The AF-CYP51A model exhibits the P450 fold and has good structural similarities in most of the regions to the MT-CYP51 crystal structure. The RMSD from the template, MT-CYP51, for all the backbone atoms is 1.59 Å. The largest deviation comes from the residues R274-L287. These residues constitute the HI loop and the N-terminal of the large I helix, which is kinked away from the structural core. The model shows two substrate access channels similar to the template MT-CYP51 and the residues forming these channels in AF-CYP51A are described below. It should be noted that the substrate access channel observed for P450cam corresponds to channel 2 of MT-CYP51. The Ramachandran plot results show 98% of residues to be distributed in the allowed, generously allowed and core regions of the plot. Only 1% of the total residues lie in the disallowed regions. Of these the non-PRO and non-GLY residues are C123, S117, N479, C314, and V315. These are predominantly surface residues. The PRO and GLY residues in allowed and disallowed regions of the plot constitute the remaining 1% of the total residues.

3.2.1. Substrate access channel 1. The bent I helix and the BC loop of the model, define a large opening (cf. channel 1 in Fig. 2) leading from the surface of the protein to the heme. Similar to MT-CYP51 crystal structure, this channel runs almost parallel to the heme. Channel 1 describes a funnel from the surface of the protein along the heme plane. The funnel narrows to a chamber lined by residues from the B′ and the I helices,

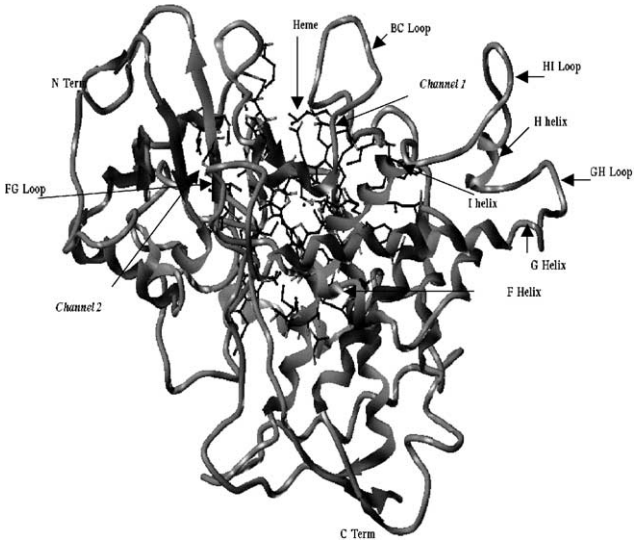

Figure 2. AF-CYP51A model showing the various secondary elements and the substrate access channels 1 and 2.

and the β-strand β1-4. Internally as the funnel broadens few residues from the I helix (A284-G294) interact with ligands. The surface of channel 1 is lined by residues from the BC loop, viz.; G116 and S117 and by D280 from the HI loop. The residues D118, D122, K273, D280, and K281 may form salt bridges, which have been shown to be electrostatically most stable and known to be involved in closing the channel upon substrate binding in the P450 family.[21–23] These salt bridges are also present at the surface of the proposed substrate access channel in P450cam.[21–23]

3.2.2. Substrate access channel 2. This channel is almost perpendicular to access channel 1 and is bounded by residues of A′ helix and the FG loop (cf. Fig. 3 and Table 3). Upon mapping to the AF- CYP51A model, it was observed that salt bridges occur only at the surface of channel 1 in AF- CYP51A and are absent among residues lining the surface of channel 2. Therefore, there exists a possibility, that in spite of the presence of two channels, the absence or presence of salt bridges at the

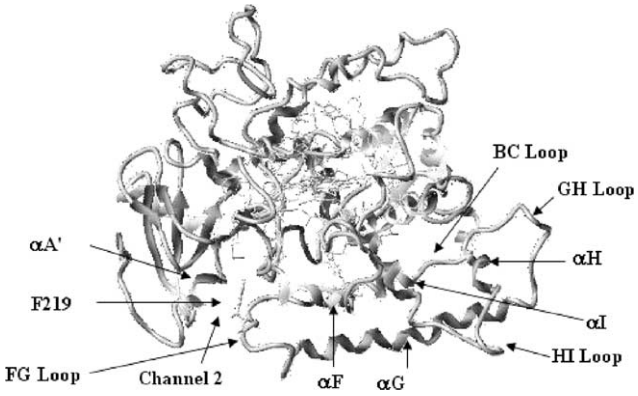

Figure 3. AF-CYP51A model showing channel 2, the FG loop, the A′ helix, and the residue F219 in the substrate access channel 2.

Table 3. Motifs lining the active site of AF-CYP51A (residues in the active site within 8 from heme are underlined and shown in bold)

Motifs	Position in sequence	Residues
B′ helix	107–115	**Y**SPLTTPVF
BC loop	116–126	GSDVVYDCPNS
C helix	127–139	K**LME**QK**KFI**KYGL
E helix	176–192	AAMAEITIFTAARA**L**QG
F helix	203–211	FADLYHDLD
G helix	229–249	NKKRDAAHARMRSIYVDIINQ
H helix	264–268	IWNLM
HI loop	269–280	NCTYKNGQQVPD
I helix	281–308	KEIAHMMIT**LLMA**G**QHS**SSS**SI**SA**W**IMLR
Loop between K helix and β1-4 strand	361–366	**HSSI**HS
Loop between β3-3 and β3-2 strands	476–505	RLFNVDGKKGVPETDYSSLF**S**GPMKPSIIG

surface may determine, which channel is functional and allows the entry of substrate and inhibitor molecules into the active site. Hence, in AF-CYP51A, the BC loop in conjunction with the HI loop may provide an entry point for all molecules, either substrate or inhibitors, accompanied by significant changes in protein conformation. The various residues defining the motifs bounding the active site as well as substrate access channels are listed in Table 3.

3.2.3. Active site of AF-CYP51A. Earlier in this study, a sequence based prediction of the active site residues has been described and these are further investigated structurally for their involvement in the active site.

Holm and Sander[24] have described propensity of amino acid residues in the active site based on how often a particular amino acid was in contact with bound ligand atoms in three-dimensional structures of proteins–ligand complexes. Based on these propensities, scores have been assigned to different amino acid residues. Positive scores mean that the amino acid makes more contacts than one would expect by chance; negative values mean that it makes fewer.[24,25] Histidine has the highest preference of 0.360, to be located within the active site of a protein. Histidines are very common in metal binding sites (e.g., Zn), often acting together with Cysteines or other amino acids. Considering this, the active site of AF-CYP51A model is a typical active site. Three histidine residues, H296, H361, H365, lie within 8 Å of the active site. Serine has a preference of 0.130 to lie in an active site and is present in abundance in the active site of AF-CYP51A model. There are seven serine residues; S297, S298, S299, S300, S302, S363, S366, which lie in the active site. The small size of serine means that it is relatively common within tight turns on the protein where it is possible for the serine side-chain hydroxyl group to form a hydrogen bond with the protein backbone, effectively mimicking proline.[25] As pointed out earlier, the S363 in AF-CYP51A is a mutation from P320 of MT-CYP51. Thus, S363 may be mimicking P320 of MT-CYP51, as a result of which the geometry is conserved, though effective cavity space is enhanced. An important feature of the AF-CYP51A model is the serine tetrad composed of S297, S298, S299, S300. This tetrad, lies on the I helix involved in ligand binding and reactivity.

Based on sequence analysis, the predicted residues that are conserved in all four gene products are Y107, E130, L190, G294, H296, S298, W304, H361 of AF-CYP51A. Of these, only Y107, L190, G294, H296, and S298 are present within 8 Å in the active site of AF-CYP51A. A structural analysis of the conserved active site residues identified through sequence analysis, viz. E141, L204, G308, H310, S312, W318, and H373 of CA-CYP51 showed that the residues were also structurally well conserved across MT-CYP51 and AF-CYP51A. The residues L139, M140, K144, F145, M306, S314 of CA-CYP51, which were conserved only across the fungal species, did not exhibit any major structural change in AF-CYP51, in spite of the change in amino acid properties. The residues A146 and M374 of CA-CYP51 mutated across all the four gene products did not bring about a conformational change, although chemically these residues have varying properties. If any of these residues is found to be predictive of activity through the COMBINE analysis (vide infra), the significance of their mutation can then be explained based on their chemical properties.

3.3. Docking of ligands

The AF-CYP51A model shows the presence of two channels as described above. These two channels contain the active site, bounded at the bottom by the porphyrin ring of heme. Azole molecules considered in the study (cf. Chart 1) were docked in the active site, with the N4 of the triazole ring forming a coordinate bond with the Fe of heme. Further, the 2,4-dihalo-phenyl ring of the ligands interacted with various residues. The receptor–ligand interactions of all ligands considered in this study are given below, however, only four complexes are shown in Figures 4–7. Other figures have been omitted due to paucity of space. Of the 10 ligands docked into the receptor, voriconazole, TAK-187, itraconazole, and ketoconazole stabilized in channel 1 (C1). On the other hand, fluconazole, SCH-43427, oxiconazole, ER-30346, compound J1-114, and sankyo, stabilized into channel 2 (C2) of the receptor. Significantly, all the long compounds docked into channel 1. This suggests that inspite of the existence of two channels, long ligands cannot explore channel 2, since there might be a block, preventing stabilization of long molecules in channel 2. This block in the form of interaction between

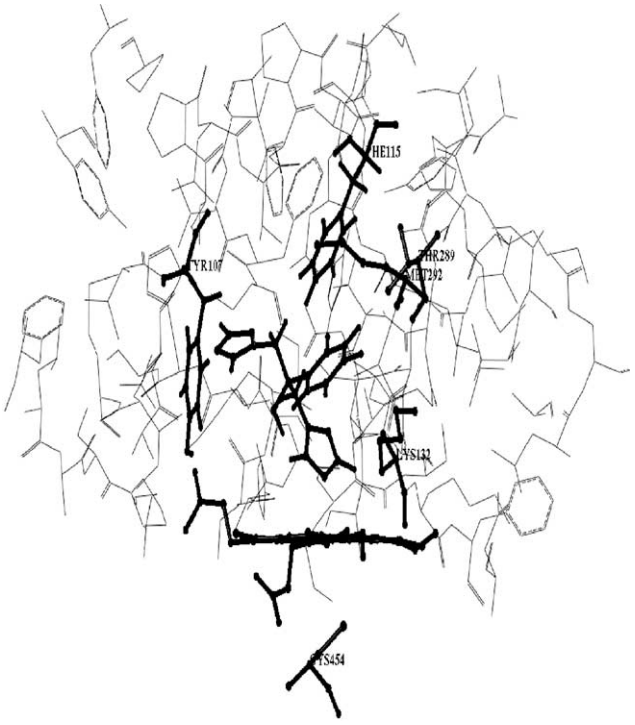

Figure 4. Docking of fluconazole in AF-CYP51A into channel 2. The residues within 8 Å from ligand in the active site are shown.

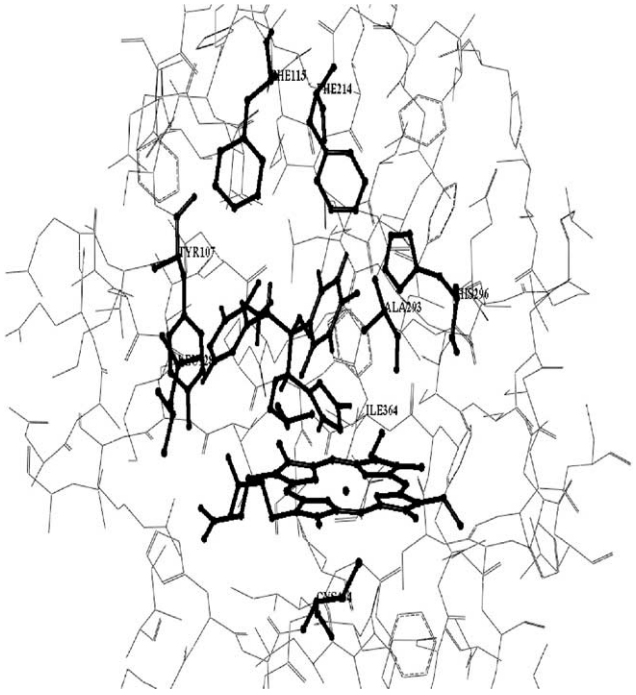

Figure 6. Docking of voriconazole in AF-CYP51A into channel 1. The residues within 8 Å from ligand in the active site are shown.

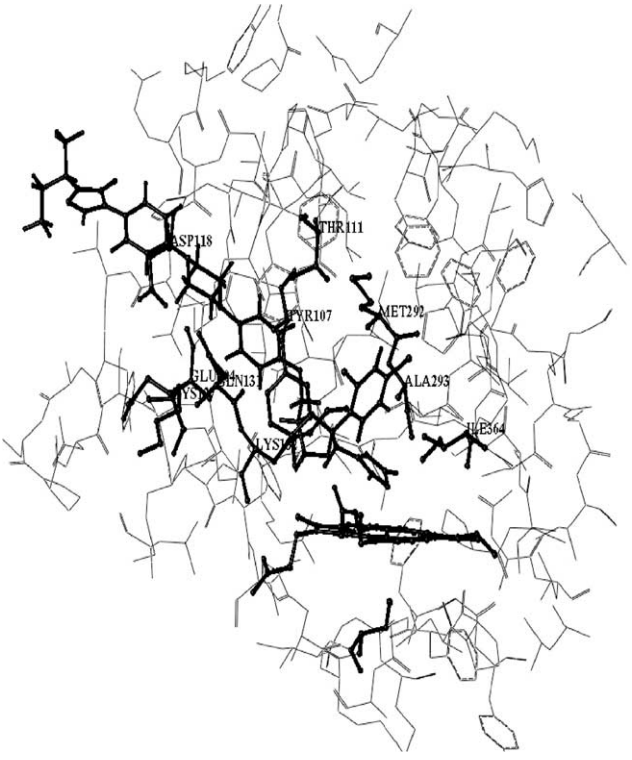

Figure 5. Docking of itraconazole in AF-CYP51A into channel 1. The residues within 8 Å from ligand in the active site are shown.

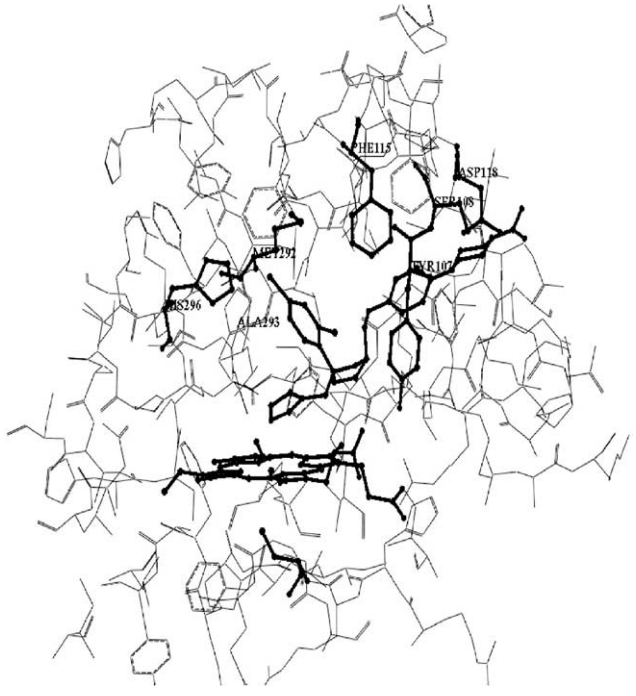

Figure 7. Docking of ketoconazole in AF-CYP51A into channel 1. The residues within 8 Å from ligand in the active site are shown.

the FG loop and the A′ helix and movement of the residue F219, on the FG loop has been described earlier.

As shown in Figure 4, the second triazole ring of fluconazole (non-Fe-binding ring) shows van der Waals interactions with the Y107. The 2-4-difluorophenyl ring of fluconazole exhibits π–π stacking with F115 of the receptor. Hydrophobic interactions exist between the fluconazole and K132, T289 and M292. The docked fluconazole superimposes three dimensionally with the

co-crystallized fluconazole in MT-CYP51 and interactions are also similar to those reported.[8] Itraconazole binds to the AF-CYP51A mainly through van der Waals interactions with residues, E104, Y107, D118, Q131, L132, and I364 (cf. Fig. 5). The N125 makes a hydrogen bond with the five-membered ketone ring of itraconazole. Hydrophobic interactions occur between K127, M292, A293, and 2,4-dichloro-phenyl ring of itraconazole. As shown in Figure 6, voriconazole exhibits π–π stacking of 2,4-difluorophenyl ring with F214 and H296 along with hydrophobic interactions with A293 and I364. The pyrimidine ring of voriconazole, shows hydrophobic interactions with Y107, F115, and L128. The aromatic ring of ketoconazole exhibits π–π stacking with F115 and van der Waals interactions are seen between the six-membered ring of ligand and S108, D118 (cf. Fig. 7). Hydrophobic interactions of the ligand exist with M292, A293, and H296. The five-membered ring having two oxygens shows van der Waals interactions with Y107.

The difluorophenyl ring of Sankyo, shows hydrophobic interactions with K132 and T289. This ring also exhibits a π–π stacking with F115, similar to docked fluconazole. The aromatic phenyl ring carrying the trifluoromethyl group interacts hydrophobically with Y107 and L494. The CF_3 group of Sankyo, shows hydrophobic interactions with I367 and M368. The methyl group of the ligand has hydrophobic interactions with T111. Compound J1-114 interacts in the following manner with the receptor: The difluorophenyl ring has hydrophobic interactions with L128, Q131, and K132. The CN group of J1-114, exhibits hydrogen bonding with Y53. Similar hydrogen bonding through CN was observed in case of thrombin and other trypsin-like proteases inhibitors.[27] The phenyl ring of benzonitrile, interacts with S366 and L494 by hydrophobic interactions. The thiophene ring of the ligand interacts hydrophobically with I364 and I367. The methyl group of J1-114 has hydrophobic interactions with L128 of the receptor. The molecule ER-30346 also shows predominantly hydrophobic interactions with the receptor. Various hydrophobic interactions between ER-30346 and receptor are; the difluorophenyl ring of ER-30346 interacts with Q131, K132, and T289. The benzonitrile ring interacts with Y107, S366, and L494. The thiazole ring of ER-30346 interacts with Y107 and I367; whereas the methyl group of ligand interacts with L128. The difluorophenyl ring also shows π–π stacking with F115. The molecule oxiconazole interacts though hydrophobic means as follows: The dichlorophenyl ring of oxiconazole interacts with M292, A293, S297. The second 2-4-phenyl ring of the ligand side chain, interacts with Y107, L110, S366, I367, and L494 of the receptor. There is π–π stacking of the dichlorophenyl ring with H296 of the receptor. Takeda's TAK-187 also shows significant hydrophobic interactions through its difluorophenyl ring with residues, M292, A293, H296, S297, and I364. The second phenyl ring with the alkoxy substituent interacts hydrophobically with Y107, K127, L128, and Q131. The methyl group has hydrophobic interactions with F115 and M292. The difluorophenyl ring of the Schering–Plough molecule SCH-42427, interacts through van der Waals interactions with F115. This ring also shows hydrophobic interactions with K132, L291, M292, and A293. The methyl group of the ligand interacts hydrophobically with L128 of the receptor; whereas the SO_2Me group on the ligand interacts hydrophobically with Y107.

Significantly, most of the above interactions of azole molecules with the active site of AF-CYP51A, are hydrophobic in nature. There is very little stabilization arising through hydrogen bonding, between ligands and the receptor. This can be explained on the basis of the largely hydrophobic nature of the active site. Analysis of docking of different ligands bring out some general trends, viz.: ligands that are stabilized in channel 1 exhibit interaction of residues M292, A293, and H296 with dihalophenyl ring of ligands; whereas this ring interacts with residues F115, K132, and M292 in channel 2. The methyl group of ligands interacts with different residues across the ligands and therefore, no common residues can be implicated in ligand binding. The common residues involved in ligand recognition irrespective of their binding either into channel C1 or C2 are, L110, T111, M292, and A293.

Table 4, lists the ligands used in this study, their reported activities (in MIC) and the corresponding binding energies after docking. Lepesheva et al.[26] have recently reported the importance of the residues Y76, F83, G84, D90, L172, G175, and R194 in the ability of MT-CYP51 to bind the substrate lanosterol. Single amino acid substitutions of these seven residues, result in loss of the ability of the mutant MTCYP51 to metabolize lanosterol. Of these seven residues, our docking analysis shows Y107, F115, L110 in AF-CYP51A, (Y76, F83, L172, in MT-CYP51A), to be involved in ligand interaction and defining receptor–ligand interactions. These residues, analogous to the MT-CYP51 structure, lie in the B′ and C helices, bounding the active site of the AF-CYP51A.

In order to establish a quantitative correlation between the binding energies and the reported ligand activities, a QSAR approach was adopted, as described in Methodology. The activity data has been expressed as $-\log(\text{MIC})$. Since activity data for ketoconazole and

Table 4. Experimental activities and binding energies of ligands shown in Chart 1

Ligand	MIC ff (μg/mL)	Binding energies (kcal/mol)
Fluconazole	>80	−13.39
Itraconazole	63	−39.10
Voriconazole	0.5	−15.71
SCH-43427	25	−50.05
ER-30346	0.8	−15.25
TAK-187	8.9	−16.18
J1-114	13	−9.99
Sankyo	22	−11.14
Oxiconazole	NA	−6.26
Ketoconazole	NA	−15.34

NA = Not available.

oxiconazole was not available eight of the ten docked molecules were considered for QSAR analysis. QSAR analysis of this data did not reveal significant correlation ($r^2 = 0.11$) between the reported ligand activities and the total binding energies. Therefore the components of binding energies viz.; steric and electrostatic have been evaluated to establish their correlation with the reported activities. Although the individual components do not have a good correlation for the entire set, the combined equation with two parameters led to a coefficient of determination (r^2) of 0.36. It was found that after removing compound ER30346 from the analysis, the statistical significance of above model improves dramatically resulting in the following equations.

$$\text{Activity} = 0.0332T_{\text{ste}} + 0.6640$$
$$n = 7, \quad r^2 = 0.61, \quad q^2 = 0.16, \quad \text{Std error} = 0.50 \quad (1)$$

$$\text{Activity} = 0.0373T_{\text{ste}} + 0.0077T_{\text{ele}} + 1.1508$$
$$n = 7, \quad r^2 = 0.77, \quad q^2 = 0.11, \quad \text{Std error} = 0.43 \quad (2)$$

where T_{ste} and T_{ele} are the steric and electrostatic components of binding energy, respectively.

Eqs. 1 and 2 show that steric contributions are dominating in this relationship, whereas there is a further improvement when the electrostatic component is also incorporated. Applying a PLS regression method to this data improves the predictive ability of the model with a q^2 of 0.31 with a single component. The Z-score q^2 value was calculated by generating 10 random sets and this value (1.39) suggested that QSAR model was better than random with 90% confidence.

3.4. COMBINE analysis

COMBINE analysis was performed by two approaches as described earlier for identifying and quantifying important residues involved in ligand interaction.

3.4.1. Approach I. Calculated descriptors and reported biological activities were subjected to various runs of stepwise multiple linear regression analysis, which has resulted in few significant equations as shown in Table 5. All the equations in Table 5 show dominance of electrostatic contributions in determining the biological activity. Equation 2 in Table 5 is the most significant, highlighting the importance of electrostatic interactions of two residues H296 and K281 with the ligand. As described earlier, residue H296 may be involved in the catalytic interactions at the active site. K281 has been hypothesized to form salt bridges at the entrance to the substrate access channel with aspartates lining the channel. This could be a tethering mechanism, which closes the channel upon binding of ligand to the active site. The obtained relationship supports the above hypotheses. The observed and q^2 predicted activity obtained from equation 2 of Table 5 is shown in Figure 8a.

Further, a PLS regression was performed using all the descriptors having a significant correlation as reported in Table 5. Using two components, the important statistical parameters obtained are; $n = 8$, $r^2 = 0.97$, Std error $= 0.165$, $q^2 = 0.84$, cv-std error $= 0.38$, and the Z-score $q^2 = 2.175$.

The PLS model shows 75% and 25% contribution of electrostatic and steric components, respectively. Figure 8b shows contribution of individual residues to the above PLS model. The resulting predicted activities as well as the residuals are shown in Table 6. Figure 8c and d show fitting of observed versus q^2 predicted and observed versus predicted activities, respectively, of the generated PLS model.

As mentioned earlier an important feature of the AF-CYP51A model is the serine tetrad composed of S297, S298, S299, and S300. To explain its significance we have performed PLS regression using electrostatic and steric energy contribution of these four residues. The PLS regression obtained shows that only electrostatic contributions play an important role in ligand binding. Using three components the important statistical parameters obtained are; $n = 8$, $r^2 = 0.92$, Std error $= 0.30$, $q^2 = 0.53$, cv-std error $= 0.74$, and the Z-score $q^2 = 1.98$. The PLS regression obtained explains the importance of the serine tetrad observed in the AF-CYP51A. This PLS model indicates that S298 has a dominating contribution (approx. 50%) of the four serines.

3.4.2. Approach II. Calculated descriptors (having variance greater than 0.01 kcal/mol) and biological activity was subjected to various runs of stepwise multiple linear regression analysis and the resulting significant equations are reported in Table 7.

Table 7 describes significance of steric contributions of three residues A293, L110, H296 and electrostatic

Table 5. Significant QSAR equations generated by COMBINE analysis Approach I

S. no	Equation	r^2	q^2	Std error
1	Activity $= -0.271\Delta E_{\text{ele}}$K127 $+ 0.166\Delta E_{\text{ste}}$H296 $- 1.058$	0.833	0.244	0.394
2	Activity $= -0.699\Delta E_{\text{ele}}$H296 $+ 2.525\Delta E_{\text{ele}}$K281 $- 1.313$	0.851	0.673	0.372
3	Activity $= 0.214\Delta E_{\text{ste}}$H296 $+ 0.292\Delta E_{ele}$E104 $- 1.439$	0.728	0.404	0.502
4	Activity $= -1.160\Delta E_{\text{ele}}$F115 $+ 0.421\Delta E_{\text{ele}}$Y107 $- 0.131$	0.601	0.153	0.609
5	Activity $= 0.278\Delta E_{\text{ele}}$E104 $+ 0.170\Delta E_{\text{ste}}$L494 $- 1.387$	0.521	0.129	0.666
6	Activity $= -0.268\Delta E_{\text{ele}}$K127 $+ 0.096\Delta E_{\text{ele}}$R369 $- 0.674$	0.576	−0.254	0.627
7	Activity $= -0.615\Delta E_{\text{ele}}$S297 $+ 0.201\Delta E_{\text{ste}}$H296 $- 2.308$	0.634	0.119	0.583

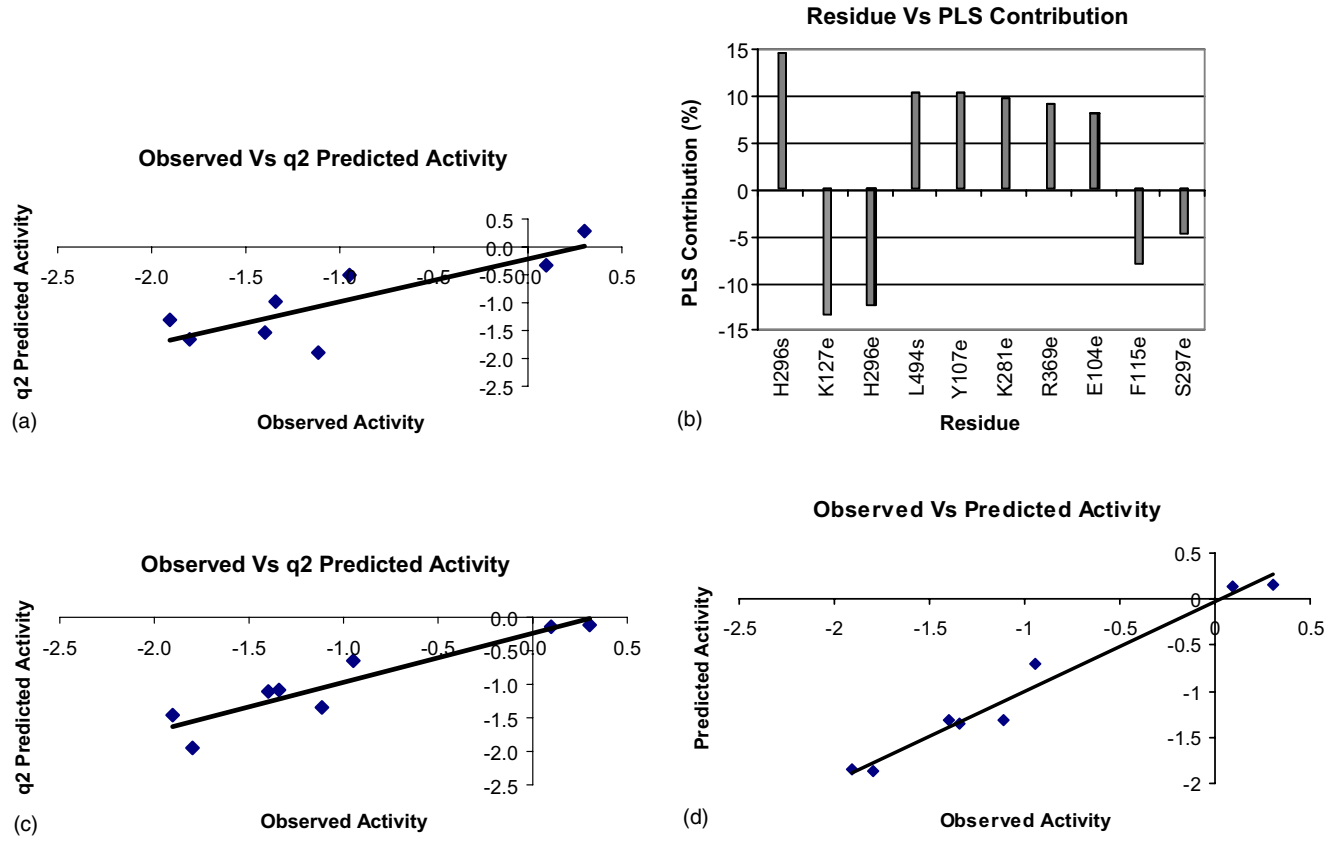

Figure 8. (a) Observed and q^2 predicted activity from equation 2 of Table 5. (b) Contributions of individual residues of PLS model using Approach I. (c) Observed and q^2 predicted activity of PLS model using Approach I. (d) Observed and predicted activity of PLS model using Approach I.

Table 6. Experimental and predicted activities of ligands using PLS model generated using Approach I of COMBINE analysis

Molecule	Observed activity	Predicted activity	Residual
ER30346	0.097	0.144	−0.047
Fluconazole	−1.903	−1.846	−0.057
Itraconazole	−1.799	−1.870	0.071
J1_114	−1.114	−1.307	0.193
Sankyo	−1.342	−1.354	0.012
SCH42427	−1.398	−1.315	−0.083
TAK187	−0.949	−0.708	−0.241
Voriconazole	0.301	0.149	0.152

interaction of Y107 in determining activity from equations 3 and 4. A293 is one of the closest residue to the bound ligands and interacts with ligands partitioning into both the channels C1 and C2. L110 lies in the region between both the channels and could be important for ligand recognition. It may be noted that the importance of A293 and L110 was not highlighted by Approach I, but has been effectively brought out by Approach II. The observed and q^2 predicted activity obtained from equation 4 of Table 7 is shown in Figure 9a.

The PLS regression obtained by the combination of above four descriptors (A293s, L110s, Y107e, H296s), from equations (3) and (4) led to the following model using two components. The important statistical parameters for this model are; $n = 8$, $r^2 = 0.95$, Std error = 0.22, $q^2 = 0.79$, cv-std error = 0.44, and the Z-score $q^2 = 1.88$.

To understand the importance of all descriptors shown in Table 7, a PLS model was generated with three

Table 7. Significant QSAR equations generated by COMBINE analysis Approach II

S. no	Equation	r^2	q^2	Std error
1	Activity $= -2.053\Delta E_{ele}$H296 $+ 0.713\Delta E_{ste}$L110 $- 1.775$	0.825	0.047	0.403
2	Activity $= -3.947\Delta E_{ele}$T289 $+ 6.401\Delta E_{ste}$K212 $- 1.587$	0.752	0.216	0.479
3	Activity $= 0.851\Delta E_{ste}$H296 $- 1.418\Delta E_{ele}$Y107 $- 1.454$	0.833	0.539	0.393
4	Activity $= -2.408\Delta E_{ste}$A293 $+ 1.027\Delta E_{ste}$L110 $- 1.302$	0.924	0.721	0.266
5	Activity $= 8.746\Delta E_{ste}$K212 $- 3.791\Delta E_{ele}$F115 $- 0.8984$	0.769	0.420	0.463
6	Activity $= -2.018\Delta E_{ste}$D118 $- 2.833\Delta E_{ele}$K127 $- 1.730$	0.496	0.019	0.684
7	Activity $= -2.052\Delta E_{ele}$K132 $- 1.803\Delta E_{ste}$D118 $- 1.075$	0.497	0.089	0.683
8	Activity $= 4.547\Delta E_{ele}$T111 $+ 7.062\Delta E_{ele}$L128 $- 0.916$	0.783	0.044	0.448

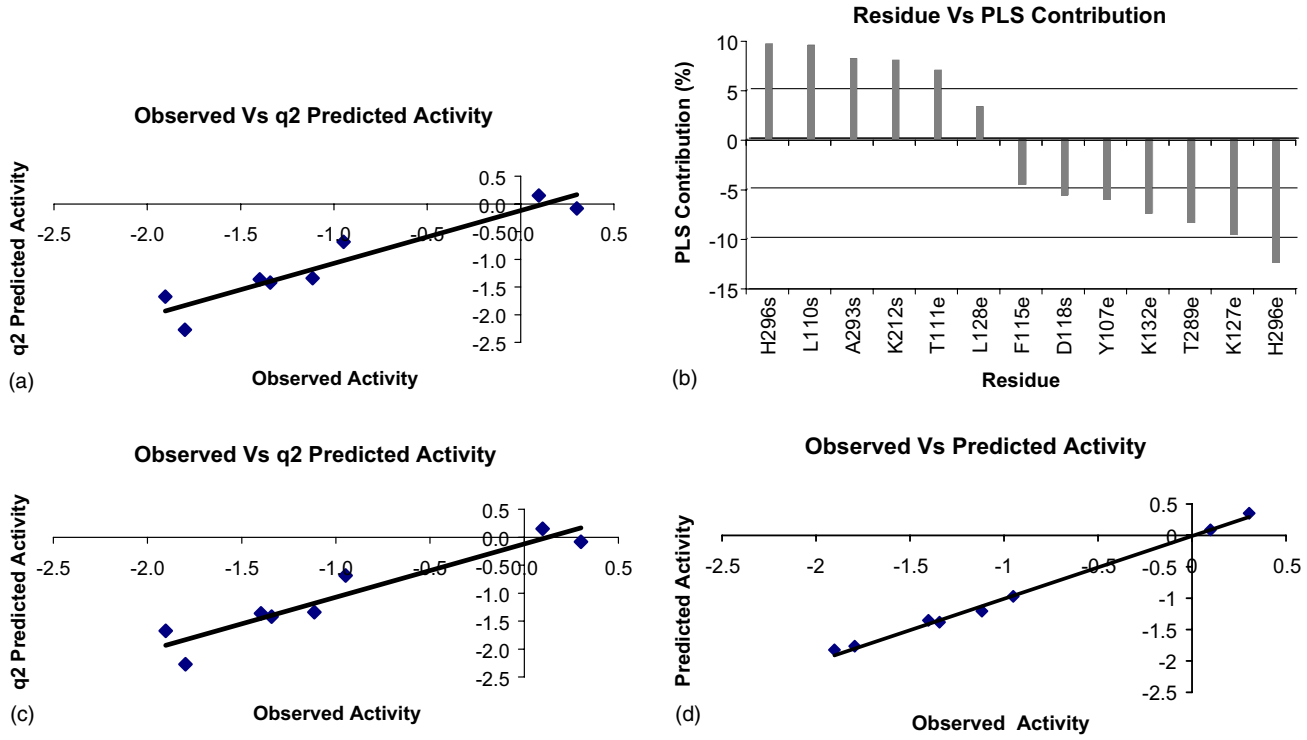

Figure 9. (a) Observed and q^2 predicted activity from equation 4 of Table 7. (b) Contributions of individual residues of PLS model using Approach II. (c) Observed and q^2 predicted activity of PLS model using Approach II. (d) Observed and predicted activity of PLS model using Approach II.

components having important statistical parameters for this model viz.; $n = 8$, $r^2 = 0.99$, Std error = 0.08, $q^2 = 0.88$, cv-std error = 0.37, and the Z-score $q^2 = 1.78$. The improvement in the model indicates importance of the remaining descriptors in addition to the four descriptors mentioned above. The individual contribution of the descriptors is shown in Figure 9b.

The PLS model shows 70% and 30% contribution of electrostatic and steric terms, respectively. A comparison of the experimental and predicted activity data by PLS model is shown in Table 8. Figure 9c and d shows fitting of observed versus q^2 predicted and observed versus predicted activities, respectively, of the generated PLS model.

It can be inferred from the PLSR coefficients (having PLS contribution around ±10%) of COMBINE analysis and individual energy contributions of voriconazole, ER-30346 and fluconazole that the interactions of the residues playing important role in activity determination have more favorable interactions (with reference to direct or inverse relation) with the residues in case of voriconazole and ER-30346. In case of fluconazole the above interactions are mostly unfavorable. This may be possible reason for high anti-*Aspergillus* activity of voriconazole and ER-30346 and low activity of fluconazole from COMBINE analysis.

Table 8. Experimental and predicted activities of ligands using PLS model generated using Approach II of COMBINE analysis

Molecule	Observed activity	Predicted activity	Residual
ER30346	0.097	0.095	0.002
Fluconazole	−1.903	−1.828	−0.075
Itraconazole	−1.799	−1.770	−0.029
J1_114	−1.114	−1.217	0.103
Sankyo	−1.342	−1.392	0.050
SCH42427	−1.398	−1.365	−0.033
TAK187	−0.949	−0.976	0.027
Voriconazole	0.301	0.344	−0.043

4. Concluding remark

A model of *A. fumigatus* lanosterol 14-α-demethylase enzyme A (CYP51A) has been built on template of CYP51 of *M. tuberculosis* (MT-CYP51). The general architecture of the present model is very similar to the MT-CYP51. The sequence analysis showed that the active site composition of fungi is different from bacteria whereas it is well conserved across fungi considered in this study. Similar to the template, the model of AF-CYP51A also exhibits two channels, almost at right angle to each other. Docking of chosen azoles reveals two distinct binding modes of azoles to AF-CYP51A. The larger molecules, viz. itraconazole and ketoconazole accommodate in to the longer channel 1 as opposed to smaller molecules like fluconazole that prefer to orient in channel 2. This differential binding of the azoles dictates the interactions of ligands with specific active site residues, the contributions of which are clearly reflected in the COMBINE analysis presented herein. The COMBINE analysis facilitates quantitative association of active site residue contributions to binding, with

the experimental activities of ligands. It also provides explanation for the activity/inactivity of different ligands for AF-CYP51A. Quantitative models generated by COMBINE analysis will aid in design of better ligands along with their activity predictions.

It is known that some azoles are only active against *Candida* sp., whereas others also act on *Aspergillus* sp. Since *A. fumigatus* has two gene products of CYP51, it is now imperative that model building and detailed analysis of AF-CYP51B should be carried out. This will facilitate comparative analysis of CYP51s from *C. albicans* and *A. fumigatus*, thereby formulating strategies for design of broad spectrum antifungals.

Acknowledgements

We are grateful to Drs. U. R. Bapat and R. S. Shetty (FDC Limited, Mumbai, India) and Mr. Avinash Marathe (MBT, Pune, India) for encouragement and support. We are thankful to FDC Limited, Mumbai, India for financial assistance.

References and notes

1. Wills, E. A.; Redinbo, M. R.; Perfect, J. R.; Poeta, M. D. New Potential Targets for Antifungal Development. *Emerg. Ther. Targets* **2000**, *4*, 1–25.
2. DiDomenico, B. Novel Antifungal Drugs. *Curr. Opin. Microbiol.* **1999**, *2*, 509–515.
3. Georgopapadakou, N. H. Antifungals Targeted to Protein Modification: Focus on Protein N-Myristoyltransferase. *Expert Opin. Inv. Drugs* **2002**, *11*, 1117–1125.
4. Tafi, A.; Costi, R.; Botta, M.; Di Santo, R.; Corelli, F.; Massa, S.; Ciacci, A.; Manetti, F.; Artico, M. Antifungal Agents. 10. New Derivatives of 1-[(Aryl)[4-aryl-1H-pyrrol-3-yl]methyl]-1H-imidazole, Synthesis, Anti-*Candida* Activity, and Quantitative Structure-Analysis Relationship Studies. *J. Med. Chem.* **2002**, *45*, 2720–2732.
5. Ji, H.; Zhang, W.; Zhou, Y.; Zhang, M.; Zhu, J.; Song, Y.; Lu, J.; Zhu, J. A Three-Dimensional Model of Lanosterol 14-Alpha Demethylase of *Candida albicans* and its Interaction with Azole Antifungals. *J. Med. Chem.* **2000**, *43*, 2493–2505.
6. Macchiarulo, A.; Costantino, G.; Fringuelli, D.; Vecchiarelli, A.; Schiaffella, F.; Fringuelli, R. J. 1,4-Benzothiazine and 1,4-Benzoxazine Imidazole Derivatives with Antifungal Activity: A Docking Study. *Bioorg. Med. Chem.* **2002**, *10*, 3415–3423.
7. Rossello, A.; Bertini, S.; Lapucci, A.; Macchia, M.; Martinelli, A.; Rapposelli, S.; Herreros, E.; Macchia, B. Synthesis, Antifungal Activity, and Molecular Modeling studies of New Inverted Oxime Ethers of Oxiconazole. *J. Med. Chem.* **2002**, *45*, 4903–4912.
8. Podust, L. M.; Poulos, T. L.; Waterman, M. R. Crystal Structure of Cytochrome P450 14-Alpha-Sterol Demethylase (CYP51) from *Mycobacterium tuberculosis* in Complex with Azole Inhibitors. *Proc. Natl. Acad. Sci. U.S.A.* **2001**, *98*, 3068–3073.
9. Mellado, E.; Diaz-Guerra, T. M.; Cuenca-Estrella, M.; Rodriguez-Tudela, J. L. Identification of Two Different 14-Alpha Sterol Demethylase-Related Genes (cyp51A and cyp51B) in *Aspergillus fumigatus* and other *Aspergillus* Species. *J. Clin. Microbiol.* **2001**, *39*, 2431–2438.
10. Thompson, J. D.; Higgins, D. G.; Gibson, T. J. CLUSTAL W: Improving the Sensitivity of Progressive Multiple Sequence Alignment Through Sequence Weighting, Position-Specific Gap Penalties and Weight Matrix Choice. *Nucleic Acids Res.* **1994**, *22*, 4673–4680.
11. Needlman, S. B.; Wunsch, C. D. A General Method Applicable to the Search for Similarities in the Amino Acid Sequences of Two Proteins. *J. Mol. Biol.* **1970**, *48*, 443–453.
12. Cuff, J. A.; Clamp, M. E.; Siddiqui, A. S.; Finlay, M.; Barton, G. J. Jpred: A Consensus Secondary Structure Prediction Server. *Bioinformatics* **1998**, *14*, 892–893.
13. TRIPOS Associates, Inc. 1699S. Hanley Road, Suite 303, St. Louis, MO 63144.
14. (a) Halgren, T. A. Merck Molecular Force Field. I. Basis, Form, Scope, Parameterization, and Performance of MMFF94. *J. Comput. Chem.* **1996**, *17*, 490–519; (b) Halgren, T. A. Merck Molecular Force Field. II. MMFF94 van der Waals and Electrostatic Parameters for Intermolecular Interactions. *J. Comput. Chem.* **1996**, *17*, 520–552; (c) Halgren, T. A. Merck Molecular Force Field. III. Molecular Geometries and Vibrational Frequencies for MMFF94. *J. Comput. Chem.* **1996**, *17*, 553–586; (d) Halgren, T. A.; Nachbar, R. B. Merck Molecular Force Field. IV. Conformational Energies and Geometries for MMFF94. *J. Comput. Chem.* **1996**, *17*, 587–615; (e) Halgren, T. A. Merck Molecular Force Field. V. Extension of MMFF94 Using Experimental Data, Additional Computational Data, and Empirical Rules. *J. Comput. Chem.* **1996**, *17*, 616–641.
15. Luthy, R.; Bowie, J. U.; Eisenberg, D. Assessment of Protein Models with Three-Dimensional Profiles. *Nature* **1992**, *356*, 83–85.
16. Bartroli, J.; Turmo, E.; Algueró, M.; Boncomte, E.; Vericat, M. L.; Conte, L.; Ramis, J.; Merlos, M.; García-Rafanell, J.; Forn, J. New Azole Antifungals. 2. Synthesis and Antifungal Activity of Heterocyclecarboxamide Derivatives of 3-Amino-2-aryl-1-azolyl-2-butanol. *J. Med. Chem.* **1998**, *41*, 1855–1868.
17. MDS 1.0, Molecular Design Suite, VLife Sciences Technologies, Pvt. Ltd. Pune, India, 2003.
18. (a) *Practical Application of Computer-Aided Drug Design*; Charifson, P., Ed.; Marcel Dekker, 1997; (b) Gilbert, N. *Statistics*; W.B. Saunders: Philadelphia, PA, 1976.
19. Entrez: http://www.ncbi.nih.nlm.gov.
20. Edlind, T. D.; Henry, K. W.; Metera, K. A.; Katiyar, S. K. *Aspergillus fumigatus* CYP51 Sequence: Potential Basis for Fluconazole Resistance. *Med. Mycol.* **2001**, *39*, 299–302.
21. Wade, R. C.; Gabdoulline, R. R.; Ludemann, S. K.; Lounnas, V. Electrostatic Steering and Ionic Tethering in Enzyme–Ligand Binding: Insights from Simulations. *Proc. Acad. Sci. Natl. U.S.A.* **1998**, *95*, 5942–5949.
22. Lüdemann, S. K.; Gabdoulline, R. R.; Lounnas, V.; Wade, R. C. Substrate Access to Cytochrome P450cam Investigated by Molecular Dynamics Simulations: An Interactive Look at the Underlying Mechanisms. http://www-z.embl-heidelberg.de:8080/ExternalInfo/wade/pub/data/IJC01/whole_IJC.html.
23. Ludemann, S. K.; Lounnas, V.; Wade, R. C. How do Substrates Enter and Products Exit the Buried Active Site of Cytochrome P450cam? 2. Steered Molecular Dynamics and Adiabatic Mapping of Substrate Pathways. *J. Mol. Biol.* **2000**, *303*, 813–830.
24. Holm, L.; Sander, C. Decision Support System for the Evolutionary Classification of Protein Structures. *Intell. Syst. Mol. Biol.* **1997**, *5*, 140–146.

25. Betts, M. J.; Russell, R. B. Amino Acid Properties and Consequences of Substitutions. In *Bioinformatics for Geneticists*; Barnes, M. R., Gray, I. C., Eds.; Wiley, 2003. http://www.russell.embl-heidelberg.de/ass/ass.html.
26. Lepesheva, G. I.; Virus, C.; Waterman, M. R. Conservation in the CYP51 Family. Role of the B' Helix/BC Loop and Helices F and G in Enzymatic Function. *Biochemistry* **2003**, *42*, 9091–9101.
27. Lee, S. L. New Inhibitors of Thrombin and other Trypsin-like Proteases: Hydrogen Bonding of an Aromatic Cyano Group with a Backbone Amide of the P1 Binding Site Replaces Binding of a Basic Side Chain. *Biochemistry* **1997**, *36*, 13180–13186.